JACS
JOURNAL OF THE AMERICAN CHEMICAL SOCIETY

Article

pubs.acs.org/JACS

A Two-Component Adhesive: Tau Fibrils Arise from a Combination of a Well-Defined Motif and Conformationally Flexible Interactions

Shengqi Xiang,[†] Natalia Kulminskaya,[†] Birgit Habenstein,[†,‡] Jacek Biernat,[§,∥] Katharina Tepper,[§,∥] Maria Paulat,[†] Christian Griesinger,[†] Stefan Becker,[†] Adam Lange,[†,⊥,#] Eckhard Mandelkow,[§,∥,7] and Rasmus Linser*[,†,8]

[†]Department NMR-Based Structural Biology, Max-Planck Institute for Biophysical Chemistry, Am Fassberg 11, 37077 Göttingen, Germany

[‡]Institut Européen de Chimie et Biologie (IECB), Université de Bordeaux/CBMN UMR5248, 2 rue Robert Escarpit, 33600 Pessac, France

[§]DZNE, German Center for Neurodegenerative Diseases, Ludwig-Erhard-Allee 2, 53175 Bonn, Germany

[∥]CAESAR Research Center, Ludwig-Erhard-Allee 2, 53175 Bonn, Germany

[⊥]Institut für Biologie, Humboldt-Universität zu Berlin, Invalidenstrasse 110, 10115 Berlin, Germany

[#]Department of Molecular Biophysics, Leibniz-Institut für Molekulare Pharmakologie (FMP), Robert-Rössle-Strasse 10, 13125 Berlin, Germany

[7]Hamburg Outstation, c/o DESY, Max-Planck-Institute for Metabolism Research, Notkestrasse 85, 22607 Hamburg, Germany

[8]Department Chemistry and Pharmacy, Ludwig-Maximilians-University Munich, Butenandtstrasse 5-13, 81377 Munich, Germany

Supporting Information

ABSTRACT: Fibrillar aggregates of Aβ and Tau in the brain are the major hallmarks of Alzheimer's disease. Most Tau fibers have a twisted appearance, but the twist can be variable and even absent. This ambiguity, which has also been associated with different phenotypes of tauopathies, has led to controversial assumptions about fibril constitution, and it is unclear to-date what the molecular causes of this polymorphism are. To tackle this question, we used solid-state NMR strategies providing assignments of non-seeded three-repeat-domain Tau^{3RD} with an inherent heterogeneity. This is in contrast to the general approach to characterize the most homogeneous preparations by construct truncation or intricate seeding protocols. Here, carbon and nitrogen chemical-shift conservation between fibrils revealed invariable secondary-structure properties, however, with inter-monomer interactions variable among samples. Residues with variable amide shifts are localized mostly to N- and C-terminal regions within the rigid beta structure in the repeat region of Tau^{3RD}. By contrast, the hexapeptide motif in repeat R3, a crucial motif for fibril formation, shows strikingly low variability of all NMR parameters: Starting as a nucleation site for monomer−monomer contacts, this six-residue sequence element also turns into a well-defined structural element upon fibril formation. Given the absence of external causes *in vitro*, the interplay of structurally differently conserved elements in this protein likely reflects an intrinsic property of Tau fibrils.

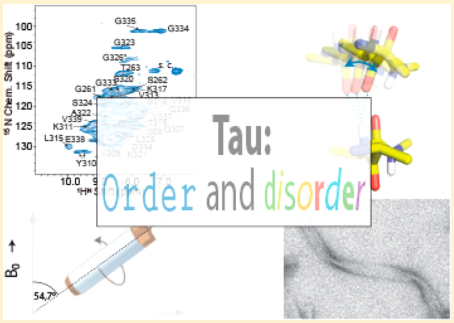

INTRODUCTION

Many proteins are able to aggregate into fibrils upon partial unfolding from a native folded state or upon partial folding from a natively unfolded state. Such fibrils are often associated with neurodegenerative diseases. However, their robust formation can also bestow organisms of different kingdoms with favorable properties (functional amyloids).[1−3] Polymorphism is found for many fibrillar aggregates.[4−7] Possible reasons for the occurrence of polymorphism are the number of protofilaments as building blocks, their relative orientation, protofilament substructure, and different interaction partners. Crystallization has been used for detailed bonding and packing studies,[7] and techniques like transmission electron microscopy (TEM) and atomic force microscopy (AFM) can define structures of full-length constructs down to atomic resolution.[8,9] Information on protofilament assembly, on secondary and tertiary structural details, and on other features, including fibrillization kinetics and interactions with chaperones, has been supplied by solution NMR[10−14] and solid-state NMR.[15−20] Unfortunately, for structure determination of protein fibrils, inhomogeneity usually needs to be eliminated by truncation and intricate seeding procedures,[21,22] even though this element in fibril properties is innate to most amyloids and represents important aspects of the nature of fibrils and their formation.

Received: September 17, 2016
Published: January 26, 2017

DOI: 10.1021/jacs.6b09619
J. Am. Chem. Soc. 2017, 139, 2639−2646

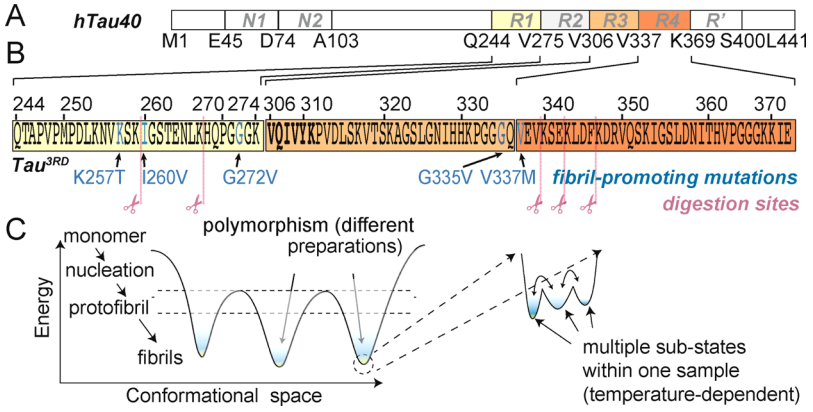

Figure 1. Architecture of the hTau40 protein. (A) The full-length isoform contains 441 amino acids consisting of four imperfect repeat domains R1−R4, flanked by Pro-rich domains N- and C-terminally. (B) Sequence of the Tau construct K19—or Tau^{3RD}—comprising the repeat domains R1, R3, and R4, with 99 amino acids. Shown are fibril-promoting mutations (blue) observed in FTDP-17 cases[49] and limited protease digestion sites (purple scissors) of Tau assembled to PHFs, pointing to the unstructured part of the K19 fibrils.[40,41] Hexapeptide residues (306−311) are shown in bold. (C) The occurrence of polymorphism as represented in a simplified energy diagram for fibril formation.

Differences in fibril structures have been correlated with differences among subtypes of neurodegenerative diseases and their severity.[23,24] For example, the amyloid plaques of Alzheimer's disease (AD) may contain different ratios of $A\beta^{1-40}$ and $A\beta,^{1-42}$ which influences fibril morphology.[6] AD is associated with these extracellular "amyloid plaques", containing mostly $A\beta$ fibrils, and dystrophic neurites containing Tau fibers. Tau fibers, which in AD associate also into intracellular "neurofibrillary tangles", have differences in constitution and morphology for the different tauopathies such as AD, Pick disease, progressive supranuclear palsy (PSP), and corticobasal degeneration (CBD).[25]

In its functional form, Tau is a soluble, intrinsically disordered protein crucial for the structure of the neuronal cytoskeleton.[26,27] Its phosphorylation-dependent[28] interaction with microtubules[29,30] defines the dynamic architecture of the cell.[31−34] The six different isoforms expressed in neurons[35] are distinguished by the presence or absence of two near-N-terminal inserts and of the second (R2) out of four imperfect, ~31-residue repeats. Thus, the repeat domain of Tau may contain either four repeats, or only three of them (called K19 or Tau^{3RD}). Repeats R2 and R3 each contain a hexapeptide motif (termed PHF6* and PHF6, respectively) that promotes fiber formation by forming cross-beta structure (Figure 1A,B).[36] Tau assembly is thought to be driven by a compensation of its positive charges, which induces a β-strand conformation with the propensity to associate with other such strands to form intra- or intermolecular sheets, and can involve interaction with additional amyloidogenic proteins like α-synuclein.[38] Also the properties of surface water around fibril core structures have recently been proposed to be a thermodynamic factor for aggregation.[39] Aggregated Tau (Figure 1C) is observed as "straight filaments" (SFs) or "paired helical filaments" (PHFs), with a width varying from 8 to 20 nm, a helix pitch of ca. 80 nm, and a so-called "fuzzy coat" around a fibril "core".[37] Limited protease digestion has been used to identify this core,[40,41] which extends roughly between residues 260 and 350 (Figure 1B). Solid-state NMR (ssNMR) has characterized the N- and C-terminal regions as water-exposed, unfolded, and dynamic.[42,43] Stacking of the cross-beta structure seems to involve in-register, parallel β-strands folded into antiparallel sheets.[44,45] Due to structural heterogeneity, no atomic-resolution ssNMR structure of this construct has been obtained yet.

The origin of the underlying Tau structural heterogeneity *in vivo* has been ascribed to various effects, including the expression of four- and three-repeat isoforms in different ratios, the possible formation of disulfide-bridged dimers as a starting point of fibril formation,[43,46] and (hyper)phosphorylation.[30] These hypotheses for *in vivo* effects have been supported by *in vitro* studies.[25] By contrast, the influence of the polyanions used *in vitro* to induce fibril formation appears to play only a minor role for differences in fibril appearance.[47] Given that different polymorphs have been associated with different subtypes of tauopathies,[23] it is tempting to ask if polymorphism is a result of merely stochastic variation or, instead, if there exist motifs inducing structural variations or conformity, respectively. If the latter, then these changes would naturally impact on the overall formation and stability of fibrils. Here we employ NMR methods to address those questions experimentally.

MATERIALS AND METHODS

Protein Expression. Uniformly (^{13}C,^{15}N)-labeled K19 C322A (Cys-free) mutant Tau^{3RD} protein was prepared as previously described.[50] Additional details are mentioned in the text and the Supporting Information (SI). This established mutant was chosen irrespective of any relevance to disease to rule out multiple peak patterns arising from differential cystein oxidation states.[43] The nomenclature used in the following (samples *A*−*D*) represents the sample described by Andronesi et al. (*A*, wt),[42] the sample used by Daebel et al. (*B*, wt),[43] and two reasonably homogeneous, recent samples (*C* and *D*, both Cys-free). Additional, non-peak-assigned preparations are shown in the SI.

NMR Spectroscopy. For resonance assignment of Tau PHFs, a combination of proton-detected and traditional, ^{13}C-detected magic angle spinning (MAS) ssNMR strategies was performed, using Bruker Avance III 800 and 850 MHz spectrometers and 1.3 and 4 mm rotors, respectively. Assignment was mostly based on hCACONH/hCOCANH experiments using four-dimensional chemical-shift encoding (Figure 2B and SI Figure 1).[48,51] Detailed information on individual sample preparation and NMR parameters, as well as 2D PDSD (SI Figure S2) and 2D NcaCB-DREAM (SI Figure S3) spectra, is available in the SI.

RESULTS

Unambiguous Chemical-Shift Assignments. Tau PHF NMR resonances are strongly heterogeneously broadened (Figure 2A). To characterize the paired helical filaments assembled from Tau^{3RD} C322A despite heterogeneity within a sample, we

DOI: 10.1021/jacs.6b09619
J. Am. Chem. Soc. 2017, 139, 2639−2646

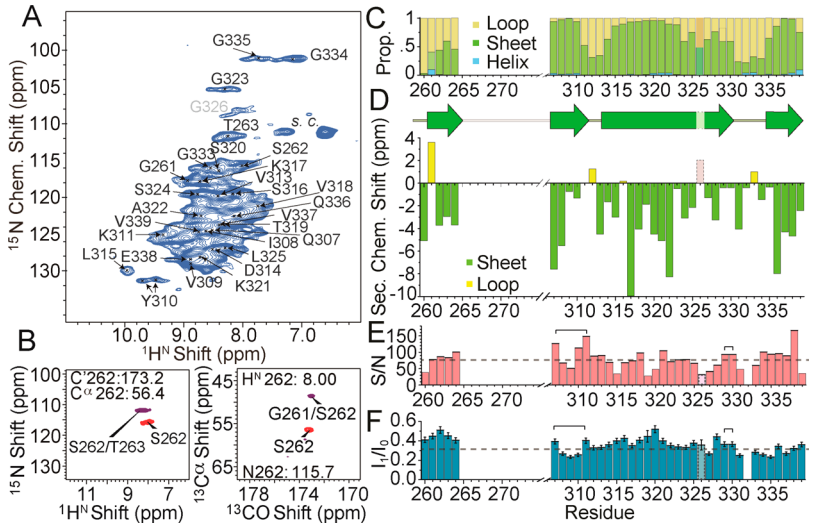

Figure 2. Assignments and directly derived protein properties of a Tau^{3RD} C322A preparation (sample *D*, which is relatively homogeneous as compared with previous studies[42,43]). (A) 2D HN correlation of 1 mg protonated fibers at 56 kHz MAS and ca. 30 °C sample temperature, annotated with assignments derived from 4D HNCACO/HNCOCA spectra. Proton resonances are strongly broadened by heterogeneity. "s.c." stands for side chain. (B) 2D slices extracted from a 4D HNCACO (magenta)/HNCOCA (purple) backbone walk, exemplified for the residues 261−263. Black labels denote third- and fourth-dimension chemical-shift values. (C) TALOS[54] propensities for the secondary-structure elements helix (blue), *β*-strand (green), and loop (beige). (D) Secondary structure derived from TALOS predictions and (below that) individual secondary chemical shifts[53] $((\delta C\alpha_{obs} - \delta C\alpha_{random}) - (\delta C\beta_{obs} - \delta C\beta_{random}))$ as a function of residue[55] (same color codes as in panel C). (E) Site-resolved peak intensity in an NCA 2D spectrum at 11 °C. (F) Site-specific water accessibility (see SI for details). Brackets in panels E and F mean the two connected residues are partly overlapping. G326 (grayed out) is a tentative assignment.

employed state-of-the-art ssNMR methods based on proton-detected experiments, supplementing standard ^{13}C-detected ssNMR spectroscopy methods. The proton-detected pulse schemes[48] employ up to four chemical-shift dimensions at up to 60 kHz MAS. Extensive and reliable ^{1}H, ^{15}N, CO, C*α*, and C*β* chemical shifts were obtained for the region between residues V306 and K340 as well as between G260 and E264 (see the SI for details). This extent is in line with limited protease digestion data.[40,41] The obtained assignments were compared with the earlier published ssNMR studies (samples *A* and *B*)[42,43] and an additional, previously unpublished assignment of K19 based on ^{13}C detection (sample *C*, see the SI for details). Secondary structural elements are very similar to those shown for residues 306−324 in the latest ssNMR study.[43] However, the unambiguous peak assignment strategy and spectral quality in four dimensions now enables highly reliable assignment and secondary-structure analysis of an extended fibril core[52] (residues 260−264 and 307−339, see Figure 2 and the SI) despite the inherent sample inhomogeneity of the unseeded preparation. Here as well as in previous studies—probably due to flexibility—sequential assignment ceases at residue V306, for which only partial and weak correlations can be obtained. Figure 2C,D shows secondary chemical shifts[53] and the invoked structural propensities of the most homogeneous sample (sample *D*) obtained as a function of residue. TALOS predictions[54] (Figure 2C) show a high *β*-strand propensity for most residues throughout the sequence, involving a central *β*-strand and shorter neighboring *β*-strand stretches. Single residues' secondary chemical shifts (Figure 2D, employing random-coil reference values predicted by ncIDP predictor[55]) slightly stand out (yellow bars), pointing to bends in the strands. These are partly associated with lower signal intensity for these residues in dipolar-coupling-based NMR experiments (Figure 2E). A water-edited experiment[42,56] (Figure 2F) shows higher water accessibility for the extended *β*-strand region between D314 and K321. Due to insufficient sequential information, G326 (shown in gray in the figures) assignments are ambiguous. The P332 ^{15}N shift is unclear due to its absence in 4D proton-detected experiments. No assignments are obtained for the 12 flexible residues between 265 and 306. This is in agreement with previous studies.[42,43]

Identification and Quantification of Fibril Polymorphism on the Basis of Chemical-Shift Comparison. Figure 3A demonstrates a selection of filament types found within a single sample (implying exactly identical conditions of formation for any fibril of the sample). Indeed, the subfields shown are taken from the same micrograph and illustrate the inherent Tau fibril polymorphism. Most significantly, the pitch varies between filaments, even though within any one fibril the structure seems consistent over many hundreds of nanometers. This macroscopic heterogeneity, however, does not necessarily lead to more than one dominant set of (broad) peaks in the NMR spectra. Solid-state NMR chemical shifts are reporters for such site-specific structural characteristics of the protein of interest. ^{13}C shifts for a given sequence are mostly dependent on secondary structure. Accordingly, the deviation of C*α* and C*β* shifts from their random-coil values, usually combined by subtraction to yield a single "secondary chemical shift",[53] is used to measure secondary-structure propensity. By contrast, ^{15}N chemical shifts of the amide backbone are sensitive to subtle changes in hydrogen bond geometry, which is sensitively affected by conformational changes of the supramolecular cross-beta arrangement. This is in contrast to such amides in flexible (non-H-bonded) elements, where ^{15}N shift changes would rather occur upon changes in pH and salt concentration (also see SI Figure 4).

Upon variation of the salt content in the fibril sample, we observe no significant change of chemical shifts, as derived from comparison of spectra before and after extensive washes of a salt-containing sample with pure water (see SI Figure 5).

DOI: 10.1021/jacs.6b09619
J. Am. Chem. Soc. 2017, 139, 2639−2646

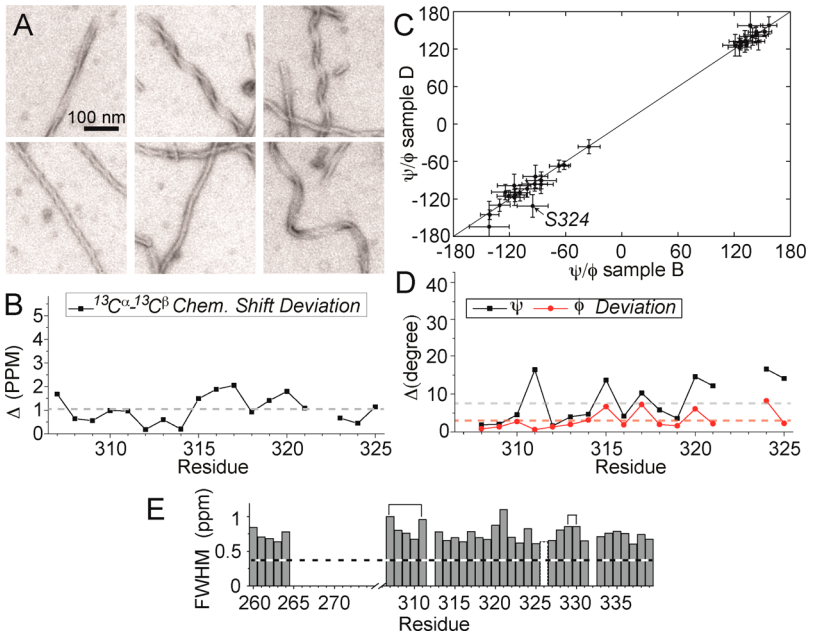

Figure 3. Fibril polymorphism and secondary structure of Cys-free Tau^{3RD}. (A) Different Tau fibrils in different areas of the same negative-stain EM picture. (B) The standard deviation of ^{13}C secondary chemical shifts in the fibril core over all four samples. For nomenclature of different samples (*A*–*D*), see Materials and Methods. (C) Example for a correlation of fibril core backbone angles between two samples, as predicted by TALOS. This plot is obtained for sample *D* (C322A) and the one in Daebel et al.[43] (sample *B*, wt). Error bars are provided by TALOS. S324 as the residue with largest deviation is annotated. See SI Figures 9–11 for a comparison between all samples. (D) Standard deviation of predicted ϕ/ψ angles in the fibril core over four samples (represented in red and black, respectively). Dashed lines denote average values. (E) $^{13}C^{\alpha}$ line widths within a single sample (using best-resolved sample *D*), read out from an NCA with long direct and indirect acquisition times. The Cα line widths shown include contributions from non-refocused $^{1}J^{CACO}$ and $^{1}J^{CACB}$ during acquisition, approximated by the dashed line. Bars connected by a line denote overlapping residues. G326 is whited out as an ambiguous assignment.

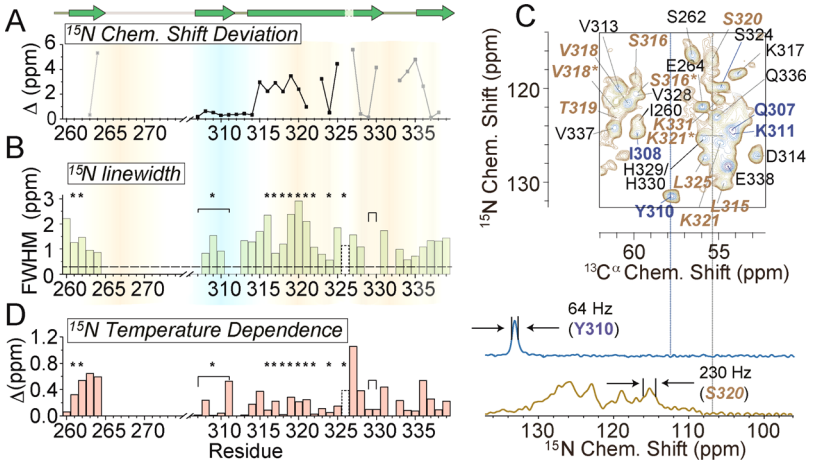

Figure 4. Site-specific ^{15}N shift differences among samples despite consistency of secondary structure motifs. (A) ^{15}N shift deviations among four different samples (*A*–*D*), combined in the form $\Delta(\text{ppm}) = \sqrt{[\sum_i (\delta_i^N - \bar{\delta}^N)^2]/n}$. Residues for which shifts from less than four data sets are available are shown in gray. Green arrows symbolize the secondary structure. (B) ^{15}N line widths (of sample *D*) as a function of residue as observed in NCA and NcaCB 2D experiments, obtained from two-dimensional peak fitting (see panel C and SI Figure 3, respectively). Bars connected by a bracket denote overlapping with other peaks in both, NCA and NcaCB spectra. The dashed line denotes the approximate contribution from homogeneous line broadening. (C) Excerpt and exemplary cross sections (including line widths) of an NCA spectrum. Shades and colored spectral annotations in panels A–C denote *particularly variable regions* (in gold/italics, with Δ(ppm) > 2 or fwhm (Hz) > 150) and residues in consecutively *homogeneous stretches* (in blue, with Δ(ppm) < 0.5). (D) Temperature variations of ^{15}N chemical shifts (Δ) between 5 and 26 °C (sample *D*). Bars connected by a line denote residues overlapping in NCA spectra. Asterisks in panels B–D denote existence of multiple peak maxima. G326 is whited out as an ambiguous assignment.

By contrast, we obtain changes in peak widths and chemical shifts for each fibril sample preparation (even if the same construct and established protocol is used). This behavior reports on variations in filament architectures in the fibrils and is in line with the negative-stain EM images described. (Larger modifications of the fibrillization procedures result in even larger spectral differences and can lead to completely non-interpretable spectra, as shown in SI Figure 12.)

DOI: 10.1021/jacs.6b09619
J. Am. Chem. Soc. 2017, 139, 2639–2646

In the case of Tau, all ssNMR assignments have been obtained without seeding.[42,43] Line widths of the inhomogeneously broadened peaks can be used for assessing inhomogeneity *within a sample*, specific to the respective nucleus employed. Taking into account the expected $^{1}J^{CACO}$ (55 Hz) and $^{1}J^{CACB}$ (35 Hz) homogeneous contributions to the line width, $^{13}C\alpha$ shifts within a single sample (sample *D*, as measured in a 2D NCA and NCACB with t_1 and t_2 of 18 and 14 ms, respectively, see Figure 3E) bear an additional inhomogeneous line width contribution on the order of 0.25 to 0.5 ppm. These ^{13}C chemical-shift properties suggest that the variations in fibril morphology observed within an individual sample are not due to (detectable) secondary structure variations.

On the other hand, also differences *between samples* are present. The largest shift differences (apart from the mutation site, C322A) are found for Cβ shifts in residue 317 (of 3.2 ppm between samples *D* and *C*), implying some changes in side chain−side chain contacts. However, different types of discrete $^{13}C-^{13}C$ peak patterns, as obtained for Aβ without seeding, are not observed (see SI Figure 6).[57] Also, secondary structure, most strongly represented by ^{13}C chemical shifts, seems to be largely consistent over different samples in different studies (see Figure 3B−D for a comparison). SI Figures 7 and 8 represent each residue's distribution of Cα and Cβ shift values over different samples. Even though differences in ^{13}C shifts between samples are obvious, the standard deviation of secondary chemical shifts over four data sets (average of around 1 ppm) is smaller than for ^{15}N shift differences (see below) and shows only weak systematic trends (Figure 3B and SI Figure 9, based on ncIDP-predicted[55] random coil values). A similarity of secondary structural features between samples is also illustrated by similar predicted backbone torsion angles (generally on the order of 10° differences between any two samples, see Figure 3C,D and SI Figures 10 and 11).

^{15}N-shift-derived site-specific fibril heterogeneity is shown in Figure 4A−C and SI Figure 8. ^{15}N shifts, which probe local conformational changes of the amide bond architecture, vary more strongly than the ^{13}C shifts. This is true both between different preparations as well as within a single batch. The latter property is represented again by the heterogeneous ^{15}N line width contributions *within one sample* (sample *D*, Figure 4B,C). Pronounced ^{15}N chemical-shift variations within a single sample (assessed via 2D peak fitting in NCA and NcaCB spectra recorded with long acquisition times, see Figure 4C and SI Figure 3) are found in the region around residues D314 to S320. Here we find broad peaks in the nitrogen dimension (up to 3 ppm inhomogeneous broadening) and/or even multiple ^{15}N maxima in the peak shape. The rest of the residues have rather well-defined peaks or only a minor degree of shift distribution (average values of around 0.5 ppm inhomogeneous broadening).

These trends are also consistent with the ^{15}N shift deviation *between samples* (see Figure 4A as well as SI Figure 8), which also report on conformational variations: We observe deviations of the peak center (RMSD over four samples) of around 3 ppm and above between 315 and 319 (and also around 325). Strikingly, however, between 307 and 314, RMSDs of consistently less than 0.5 ppm are observed for a stretch of eight consecutive residues. Interestingly, this region of little heterogeneity still belongs to a β-strand region and coincides with the hexapeptide 306−311 identified as the driving force for fibrilization in aggregation studies (see Discussion).[36] In Figure 4, "variable regions" (Δ > 2 ppm or fwhm > 2 ppm) are represented by shades and spectral annotations in gold/italics, while residues in consecutively "homogeneous stretches" (Δ < 0.5 ppm) are highlighted in blue. Figure 4D displays the temperature-induced chemical-shift differences of amide ^{15}N for a preparation of Tau^{3RD} C322A for 26 °C vs 5 °C as a function of residue number (see details in SI Figure 13).

DISCUSSION

The structural variability that is observed in this study can be related to neither co-expression of different splicing variants nor differences in post-translational modifications. The tendency for structural heterogeneity thus seems to be an intrinsic feature of the Tau protein itself rather than due to external reasons. There are several potential causes that would lead to chemical shift differences between different kinds of fibrils (see SI Figure 4 for a graphical illustration and the Supplementary Movie for an animation): (i) Solvent−Tau interactions (differences in pH/buffer/salt content etc.) should be associated with non-H-bonded amides affected more than those in the sheets. Given that a wash of the fibrils with pure water (pH 7, no salt) resulted in no spectral differences (see SI Figure 5), this is improbable. (ii) Differently bent structures (changes within the monomer geometry) would cause major ^{13}C resonance differences. Similarly, also differences in the pattern of contacts between side chains (as required by different protofilament structure, for instance C_2 vs C_3 symmetry like in Aβ) would again imply major ^{13}C shift differences. Instead, even though differences in ^{13}C shifts, including Cβ shifts, are present, we find that ^{13}C chemical shifts are more consistent than ^{15}N shifts. (iii) By contrast, different alignment of the stacked monomers within the protofilaments, implying variability in the intermolecular H-bond geometries between monomers as known for intramolecular sheets,[58,59] would result in ^{15}N shift variability in sheet regions as the major effect. Non-H-bonded ^{15}N's as well as ^{13}C secondary chemical shifts would be largely unaffected. These are the major tendencies that we observe in our study, even though alterations in side-chain contacts (assessed here only via Cβ shifts) and slight variations in backbone torsion angles are not totally absent.

This study shows that, in the "rigid core", there are certain well-defined structural features, but this structural conformity varies along the primary sequence. The region 307−314 in the central β-strand shows very high conformity in various parameters assessed in the current study. Interestingly, this region coincides with the "hexapeptide motif" PHF6, which is one binding site of Tau to microtubules and is present in all Tau isoforms. The hexapeptide has also been described as the strongest interaction site between Tau monomers/dimers under non-polymerizing conditions.[36] The high conformational definition of the PHF6 residues within fibrils observed here represents a good match with the proposition that the hexapeptide region acts as nucleation site crucial for fibril formation.[36] Adopting and maintaining a certain, well-defined structure, it functions like an adhesive to stick Tau monomers together as one of the driving events in fibril formation. The feature of PHF6 to harbor structure of highest conservation will be of significance for the search of hotspots for pharmacological treatment. This might include localization of inhibitor binding sites or identification of critical post-translational modifications to prevent Tau aggregation or other detrimental interactions. Figure 5A sketches the distribution of conserved and variable structural features in Tau fibrils. Figure 5B shows the possible

DOI: 10.1021/jacs.6b09619
J. Am. Chem. Soc. 2017, 139, 2639−2646

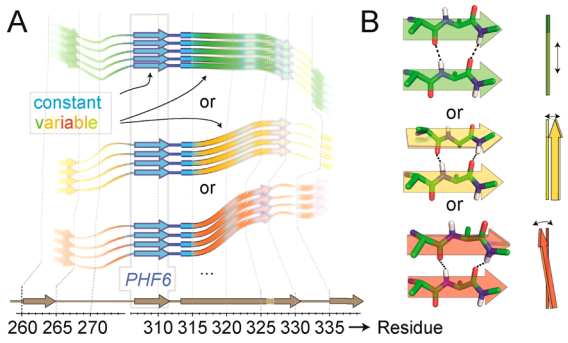

Figure 5. Pictorial interpretation of how the NMR shifts from invariable and variable residues may originate in the fibril building block. (A) Secondary structure (β-strand or loop/kink, as derived from ^{13}C secondary chemical shifts) is comparable among different batches of samples; however, ^{15}N chemical shifts of many regions ("non-blue") vary between different fibrils (see Figures 3 and 4). This hints to variability of the local chemical environment, including H-bond architecture. B) A possible explanation would be slightly different arrangement of strands with respect to each other, like slight lateral differences in relative position (top), tilt (middle), or twist (bottom example), thus creating variations of the amide ^{15}N shifts as well as supramolecular structure (right). Variability in the amide bond architecture is known from globular proteins to be associated with a large variety of possible β-sheet conformations, including shearing, twisting, and bending of β-sheets.[58,59] The hexapeptide region PHF6 (residues 306−311, blue), by contrast, has a highly conserved structure among different fibrils. Note that the simplified single-layer, elongated fold here is used for illustration of secondary structure, and variability of backbone chemical environment and structural differences are probably exaggerated. Straight shapes or a hairpin or β-helix[44] as the basic fold would be possible. The data here do not tell us about side-chain interactions.

effects that would lead to amide shift variability despite conserved secondary structure N- and C-terminal of the hexapeptide region (also see an animation in the SI).

The exact effects on macroscopic morphology remain less clear. Fibrils consisting of only the stretch N265-E338ΔR2 (PHF43) have been detected by EM to be in a straight shape, whereas polymorphic helical filaments are usually obtained when K19 or the full-length sequence is expressed.[36] We could show here that ^{15}N shift multiplicity and shift variation are more dominant in the non-hexapeptide stretches of the sequence, such that the morphologic differences (e.g., fibril pitch) might be caused by residues outside the core, thus affecting the more exterior rigid-core residues of variable geometry. However, morphology distributions (in EM) *between samples* are unknown, and compared with the very low RMSD of ^{15}N peak (center) positions between samples, line widths within the hexapeptide region are not totally devoid of heterogeneous contributions, such that a fully conclusive answer cannot be given here.

Elucidation of the exact molecular structure of a Tau conformer will require unambiguous measurement of interatomic distances in a well-ordered ensemble. The use of a dedicated aggregation agent, in this case heparin, has been indispensable for Tau fibrillization in *in vitro* studies.[39,40,42,43,47,50] Given the morphological similarity of artificial and physiological Tau fibrils as well as the success of Tau *in vitro* studies under exactly these conditions to gain insight into protein-intrinsic properties of Tau in numerous studies previously, one should assume that the structural tendencies found under such conditions indeed represent properties of the specific protein sequence. Nevertheless, the conditions of the disease case, where the cofactors for aggregation could be for example nucleic acids, acidic proteins or other unknown conditions, are hardly reproducible *in vitro*, which naturally limits the generality of this study, and any observations might be influenced by the aggregation agent employed. Consequently, the protein structural properties observed here can only be interpreted as likely tendencies for the protein *in vivo*.

The higher homogeneity of the hexapeptide region in the center of the core coinciding with its role as the main interaction site upon fibril formation raises the general question about the role of variable residues for fibril formation. Features allowing the formation of the (enthalpically favorable) intermolecular sheets without the necessity of a specific structure might attribute resilience of fibril formation against variability of the environment (pH, salt, temperature, and other protein interaction partners) as well as the existing variability within the elongating protomers (different splicing variants, post-translational modification patterns). Such properties would add a further thermodynamic or kinetic drive for aggregation and potentially represent a factor for the unfortunate evolutionary success of fibril formation as a robust protein fold, especially in neurodegenerative disease. This is, however, speculative, and individual sequence-specific features may well impose different scenarios for different proteins.

CONCLUSION

We have shown that paired helical filaments of the construct Tau^{3RD} inherently exist as an ensemble of structures. Most dominantly, amide architecture, the chemical shifts of which differ for different geometries of H-bonding interactions, varies between fibrils. However, the hexapeptide motif has a well-defined structure consistent among otherwise heterogeneous fibrils. These features may help us to understand the formation process and should inform on possibilities for future pharmacological intervention.

ASSOCIATED CONTENT

Supporting Information

The Supporting Information is available free of charge on the ACS Publications website at DOI: 10.1021/jacs.6b09619.

Experimental details, NMR spectra, chemical shift tables, and additional comparative data, including SI Figures 1−13 and Tables S1−S3 (PDF)

Supplementary movie, showing an animated representation of differences in Tau structure that would explain the NMR data obtained (MPG)

AUTHOR INFORMATION

Corresponding Author

*rasmus.linser@lmu.de

ORCID

Rasmus Linser: 0000-0001-8983-2935

Notes

The authors declare no competing financial interest.

ACKNOWLEDGMENTS

We are grateful for negative-stain EM pictures recorded by Dietmar Riedel and technical support by Brigitta Angerstein, Claudia Schwiegk, and Sabrina Huebschmann. R.L. acknowledges a Liebig fellowship (Funds of the Chemical Industries,

DOI: 10.1021/jacs.6b09619
J. Am. Chem. Soc. 2017, 139, 2639−2646

FCI) and support by the German Research Association (DFG, Emmy Noether program) and CIPSM; E.M. acknowledges support by DZNE, MPG, and Wellcome Trust/MRC; and A.L. acknowledges support by the DFG (Emmy Noether program).

REFERENCES

(1) Pulawski, W.; Ghoshdastider, U.; Andrisano, V.; Filipek, S. *Appl. Biochem. Biotechnol.* **2012**, *166*, 1626.
(2) Sunde, M.; Kwan, A. H.; Templeton, M. D.; Beever, R. E.; Mackay, J. P. *Micron* **2008**, *39*, 773.
(3) Chiti, F.; Dobson, C. M. *Annu. Rev. Biochem.* **2006**, *75*, 333.
(4) Goldsbury, C. S.; Cooper, G. J.; Goldie, K. N.; Müller, S. A.; Saafi, E. L.; Gruijters, W. T. M.; et al. *J. Struct. Biol.* **1997**, *119*, 17.
(5) Pedersen, J. S.; Dikov, D.; Flink, J. L.; Hjuler, H. A.; Christiansen, G.; Otzen, D. E. *J. Mol. Biol.* **2006**, *355*, 501.
(6) Kodali, R.; Williams, A. D.; Chemuru, S.; Wetzel, R. *J. Mol. Biol.* **2010**, *401*, 503.
(7) Colletier, J.-P.; Laganowsky, A.; Landau, M.; Zhao, M.; Soriaga, A. B.; Goldschmidt, L.; Flot, D.; Cascio, D.; Sawaya, M. R.; Eisenberg, D. *Proc. Natl. Acad. Sci. U. S. A.* **2011**, *108*, 16938.
(8) Wegmann, S.; Medalsy, I. D.; Mandelkow, E.; Müller, D. J. *Proc. Natl. Acad. Sci. U. S. A.* **2013**, *110*, E313.
(9) Schmidt, A.; Annamalai, K.; Schmidt, M.; Grigorieff, N.; Fändrich, M. *Proc. Natl. Acad. Sci. U. S. A.* **2016**, *113*, 6200.
(10) Carulla, N.; Caddy, G. L.; Hall, D. R.; Zurdo, J.; Gairí, M.; Feliz, M.; Giralt, E.; Robinson, C. V.; Dobson, C. M. *Nature* **2005**, *436*, 554.
(11) Knowles, T. P. J.; Waudby, C. A.; Devlin, G. L.; Cohen, S. I. A.; Aguzzi, A.; Vendruscolo, M.; Terentjev, E. M.; Welland, M. E.; Dobson, C. M. *Science* **2009**, *326*, 1533.
(12) Fawzi, N. L.; Ying, J.; Ghirlando, R.; Torchia, D. A.; Clore, G. M. *Nature* **2011**, *480*, 268.
(13) Karagöz, G. E.; Duarte, A. M. S.; Akoury, E.; Ippel, H.; Biernat, J.; Luengo, T. M.; Radli, M.; Didenko, T.; Nordhues, B. A.; Veprintsev, D. B.; Dickey, C. A.; Mandelkow, E.; Zweckstetter, M.; Boelens, R.; Madl, T.; Rudiger, S. G. D. *Cell* **2014**, *156*, 963.
(14) Gandhi, N. S.; Landrieu, I.; Byrne, C.; Kukic, P.; Amniai, L.; Cantrelle, F.-X.; Wieruszeski, J.-M.; Mancera, R. L.; Jacquot, Y.; Lippens, G. *Angew. Chem., Int. Ed.* **2015**, *54*, 6819.
(15) Paravastu, A. K.; Leapman, R. D.; Yau, W. M.; Tycko, R. *Proc. Natl. Acad. Sci. U. S. A.* **2008**, *105*, 18349.
(16) Wasmer, C.; Lange, A.; Van Melckebeke, H.; Siemer, A. B.; Riek, R.; Meier, B. H. *Science* **2008**, *319*, 1523.
(17) Nielsen, J. T.; Bjerring, M.; Jeppesen, M. D.; Pedersen, R. O.; Pedersen, J. M.; Hein, K. L.; Vosegaard, T.; Skrydstrup, T.; Otzen, D. E.; Nielsen, N. C. *Angew. Chem., Int. Ed.* **2009**, *48*, 2118.
(18) Lopez del Amo, J.-M.; Schmidt, M.; Fink, U.; Dasari, M.; Fändrich, M.; Reif, B. *Angew. Chem., Int. Ed.* **2012**, *51*, 6136.
(19) Fitzpatrick, A. W. P.; Debelouchina, G. T.; Bayro, M. J.; Clare, D. K.; Caporini, M. A.; Bajaj, V. S.; Jaroniec, C. P.; Wang, L.; Ladizhansky, V.; Müller, S. A.; MacPhee, C. E.; Waudby, C. A.; Mott, H. R.; De Simone, A.; Knowles, T. P. J.; Saibil, H. R.; Vendruscolo, M.; Orlova, E. V.; Griffin, R. G.; Dobson, C. M. *Proc. Natl. Acad. Sci. U. S. A.* **2013**, *110*, 5468.
(20) Tuttle, M. D.; Comellas, G.; Nieuwkoop, A. J.; Covell, D. J.; Berthold, D. A.; Kloepper, K. D.; Courtney, J. M.; Kim, J. K.; Barclay, A. M.; Kendall, A.; Wan, W.; Stubbs, G.; Schwieters, C. D.; Lee, V. M. Y.; George, J. M.; Rienstra, C. M. *Nat. Struct. Mol. Biol.* **2016**, *23*, 409.
(21) Wälti, M. A.; Ravotti, F.; Arai, H.; Glabe, C. G.; Wall, J. S.; Böckmann, A.; Güntert, P.; Meier, B. H.; Riek, R. *Proc. Natl. Acad. Sci. U. S. A.* **2016**, *113*, E4976.
(22) Colvin, M. T.; Silvers, R.; Ni, Q. Z.; Can, T. V.; Sergeyev, I.; Rosay, M.; Donovan, K. J.; Michael, B.; Wall, J.; Linse, S.; Griffin, R. G. *J. Am. Chem. Soc.* **2016**, *138*, 9663.
(23) Eisenberg, D.; Jucker, M. *Cell* **2012**, *148*, 1188.
(24) Lu, J. X.; Qiang, W.; Yau, W. M.; Schwieters, C. D.; Meredith, S. C.; Tycko, R. *Cell* **2013**, *154*, 1257.
(25) Furukawa, Y. In *Bio-nanoimaging. Protein Misfolding and Aggregation*; Uversky, V. N., Lyubchenko, Y. L., Eds.; Academic Press: Amsterdam, 2014; p 213.
(26) Lee, G.; Cowan, N.; Kirschner, M. *Science* **1988**, *239*, 285.
(27) Mandelkow, E.; Mandelkow, E.-M. *Curr. Opin. Cell Biol.* **1995**, *7*, 72.
(28) Mair, W.; Muntel, J.; Tepper, K.; Tang, S.; Biernat, J.; Seeley, W. W.; Kosik, K. S.; Mandelkow, E.; Steen, H.; Steen, J. A. *Anal. Chem.* **2016**, *88*, 3704.
(29) Sillen, A.; Barbier, P.; Landrieu, I.; Lefebvre, S.; Wieruszeski, J. M.; Leroy, A.; Peyrot, V.; Lippens, G. *Biochemistry* **2007**, *46*, 3055.
(30) Biernat, J.; Gustke, N.; Drewes, G.; Mandelkow, E. M.; Mandelkow, E. *Neuron* **1993**, *11*, 153.
(31) Hong, M.; Zhukareva, V.; Vogelsberg-Ragaglia, V.; Wszolek, Z.; Reed, L.; Miller, B. I.; Geschwind, D. H.; Bird, T. D.; McKeel, D.; Goate, A.; Morris, J. C.; Wilhelmsen, K. C.; Schellenberg, G. D.; Trojanowski, J. Q.; Lee, V. M. Y. *Science* **1998**, *282*, 1914.
(32) Sibille, N.; Huvent, I.; Fauquant, C.; Verdegem, D.; Amniai, L.; Leroy, A.; Wieruszeski, J.-M.; Lippens, G.; Landrieu, I. *Proteins: Struct., Funct., Genet.* **2012**, *80*, 454.
(33) Gigant, B.; Landrieu, I.; Fauquant, C.; Barbier, P.; Huvent, I.; Wieruszeski, J.-M.; Knossow, M.; Lippens, G. *J. Am. Chem. Soc.* **2014**, *136*, 12615.
(34) Kadavath, H.; Hofele, R. V.; Biernat, J.; Kumar, S.; Tepper, K.; Urlaub, H.; Mandelkow, E.; Zweckstetter, M. *Proc. Natl. Acad. Sci. U. S. A.* **2015**, *112*, 7501.
(35) Goedert, M.; Spillantini, M. G.; Jakes, R.; Rutherford, D.; Crowther, R. A. *Neuron* **1989**, *3*, 519.
(36) von Bergen, M.; Friedhoff, P.; Biernat, J.; Heberle, J.; Mandelkow, E.-M.; Mandelkow, E. *Proc. Natl. Acad. Sci. U. S. A.* **2000**, *97*, 5129.
(37) Crowther, T.; Goedert, M.; Wischik, C. M. *Ann. Med.* **1989**, *21*, 127.
(38) Giasson, B. I.; Forman, M. S.; Higuchi, M.; Golbe, L. I.; Graves, C. L.; Kotzbauer, P. T.; Trojanowski, J. Q.; Lee, V. M. Y. *Science* **2003**, *300*, 636.
(39) Fichou, Y.; Schirò, G.; Gallat, F.-X.; Laguri, C.; Moulin, M.; Combet, J.; Zamponi, M.; Härtlein, M.; Picart, C.; Mossou, E.; Lortat-Jacob, H.; Colletier, J.-P.; Tobias, D. J.; Weik, M. *Proc. Natl. Acad. Sci. U. S. A.* **2015**, *112*, 6365.
(40) von Bergen, M.; Barghorn, S.; Muller, S. A.; Pickhardt, M.; Biernat, J.; Mandelkow, E. M.; Davies, P.; Aebi, U.; Mandelkow, E. *Biochemistry* **2006**, *45*, 6446.
(41) Jakes, R.; Novak, M.; Davison, M.; Wischik, C. M. *EMBO J.* **1991**, *10*, 2725.
(42) Andronesi, O. C.; von Bergen, M.; Biernat, J.; Seidel, K.; Griesinger, C.; Mandelkow, E.; Baldus, M. *J. Am. Chem. Soc.* **2008**, *130*, 5922.
(43) Daebel, V.; Chinnathambi, S.; Biernat, J.; Schwalbe, M.; Habenstein, B.; Loquet, A.; Akoury, E.; Tepper, K.; Müller, H.; Baldus, M.; Griesinger, C.; Zweckstetter, M.; Mandelkow, E.; Vijayan, V.; Lange, A. *J. Am. Chem. Soc.* **2012**, *134*, 13982.
(44) Margittai, M.; Langen, R. *Proc. Natl. Acad. Sci. U. S. A.* **2004**, *101*, 10278.
(45) Margittai, M.; Langen, R. *J. Biol. Chem.* **2006**, *281*, 37820.
(46) Schweers, O.; Mandelkow, E. M.; Biernat, J.; Mandelkow, E. *Proc. Natl. Acad. Sci. U. S. A.* **1995**, *92*, 8463.
(47) Barghorn, S.; Mandelkow, E. *Biochemistry* **2002**, *41*, 14885.
(48) Xiang, S.; Biernat, J.; Mandelkow, E.; Becker, S.; Linser, R. *Chem. Commun.* **2016**, *52*, 4002.
(49) Wolfe, M. S. *J. Biol. Chem.* **2009**, *284*, 6021.
(50) Barghorn, S.; Biernat, J.; Mandelkow, E. *Methods Mol. Biol.* **2005**, *299*, 35.
(51) Xiang, S.; Chevelkov, V.; Becker, S.; Lange, A. *J. Biomol. NMR* **2014**, *60*, 85.
(52) The definition of the core varies slightly between the techniques used. Here we refer to the part of the protein from which ssNMR cross-polarization spectra (requiring reasonably rigid residues) can be derived.

DOI: 10.1021/jacs.6b09619
J. Am. Chem. Soc. 2017, 139, 2639−2646

(53) Luca, S.; Filippov, D. V.; van Boom, J. H.; Oschkinat, H.; de Groot, H. J. M.; Baldus, M. *J. Biomol. NMR* **2001**, *20*, 325.
(54) Shen, Y.; Delaglio, F.; Cornilescu, G.; Bax, A. *J. Biomol. NMR* **2009**, *44*, 213.
(55) Tamiola, K.; Acar, B.; Mulder, F. A. *J. Am. Chem. Soc.* **2010**, *132*, 18000.
(56) Kumashiro, K. K.; Schmidt-Rohr, K.; Murphy, O. J., III; Ouellette, K. L.; Cramer, W. A.; Thompson, L. K. *J. Am. Chem. Soc.* **1998**, *120*, 5043.
(57) Tycko, R. *Protein Sci.* **2014**, *23*, 1528−1539.
(58) Weatherford, D. W.; Salemme, F. R. *Proc. Natl. Acad. Sci. U. S. A.* **1979**, *76*, 19.
(59) Salemme, F. R. *Prog. Biophys. Mol. Biol.* **1983**, *42*, 95.

DOI: 10.1021/jacs.6b09619
J. Am. Chem. Soc. 2017, 139, 2639−2646